Kinetics and Catalysis, Vol. 42, No. 5, 2001, pp. 583–593. Translated from Kinetika i Kataliz, Vol. 42, No. 5, 2001, pp. 645–656.

Kinetics of Carbon Cluster Formation in the Course of C_3O_2 Pyrolysis

H. Gg. Wagner*, P. A. Vlasov, K. J. Dorge*, A. V. Eremin***, I. S. Zaslonko†**, and D. Tanke***

** Institut für Physikalische Chemie, Georg–August Universität, Göttingen, Germany*

*** Semenov Institute of Chemical Physics, Russian Academy of Sciences, Moscow, 117977 Russia*

**** Scientific Research Center for Thermophysics of Pulse Action, Joint Institute for High Temperatures, Russian Academy of Sciences, Moscow, 127412 Russia*

Received February 18, 2000

Abstract—The kinetics of the formation of condensed carbon particles in the thermal decomposition of C_3O_2 molecules behind shock waves was experimentally studied at temperatures of 1200–2500 K, pressures of ~20–60 atm, and molar fractions of C_3O_2 in a mixture with argon in the range 0.03–2.00%. The concentration of condensed carbon particles was measured by the absorption of laser radiation at wavelengths of 632.8 and 1064 nm. The experimental results were compared with data calculated in the framework of three different models. Two of these models (analytical) include the kinetics of the formation of the particle-size distribution function and give a simplified description of the kinetics of gas-phase reactions involving C_3O_2 and decomposition fragments. The third model (numerical) combines detailed descriptions of the kinetics and the coagulation dynamics. Several types of condensed carbon particles were considered: carbon clusters, soot particles, and fullerenes. The transitions between various forms of condensed carbon particles were included into the kinetic scheme of the model. All main observed specific features of the growth kinetics of condensed carbon particles during C_3O_2 pyrolysis can be described in terms of these models.

INTRODUCTION

The advantages of a shock wave technique for studying the kinetics of formation of condensed carbon during hydrocarbon pyrolysis were discussed in detail in several works [1, 2]. A number of kinetic models were proposed, which allow, with different degrees of detail, the interpretation of experimental data on the kinetics of soot formation in the pyrolysis of hydrocarbons. The so-called HACA (Hydrogen Abstraction, Acetylene Addition) model is most popular [3]. Its main idea can be reduced to the following: the addition of a C_2H_2 molecule (as assumed, C_2H_2 molecules are the main "building material" in soot growth) to a soot nucleus results in the escape of H atoms to the bulk, and they provide the further development of a chain reaction. The so-called "whole model" of soot formation was also developed [4, 5], which can describe available experimental data on soot formation during hydrocarbon pyrolysis.

The great interest in soot formation specifically in hydrocarbon systems is understandable and results mainly from applied aspects of the problem. At the same time, other classes of compounds are of considerable interest from the fundamental point of view. The use of these compounds could reveal more reliably the main factors determining the kinetics of growth of condensed carbon particles. These concepts have been developed in several recent works. Thienel [6] examined the kinetics of soot growth during the pyrolysis of completely fluorinated hydrocarbons. The observed kinetic parameters for soot growth were found to be only slightly different from those measured in the pyrolysis of hydrocarbons.

Starikovskii *et al.* [7] studied the kinetics of soot formation in the pyrolysis of CCl_4 in argon and CCl_4–H_2 and CCl_4–$Fe(CO)_5$ binary mixtures. We briefly consider only the results obtained for the CCl_4–H_2 mixture. This system is interesting because C atoms and small C_2 and C_3 particles predominate, at least at early stages of the processes. They are formed in the fast reactions

$$CCl_4 \longrightarrow \dot{C}Cl_3 + Cl,$$

$$Cl + H_2 \longrightarrow HCl + H,$$

$$H + \dot{C}Cl_x \longrightarrow HCl + \dot{C}Cl_{x-1} \quad (x = 1\text{–}4),$$

and "strip" the chlorine shells of $\dot{C}Cl_x$ particles. As a result, the formation of condensed carbon becomes much easier and leads, in particular, to a shift of the lower temperature boundary of the appearance of carbon clusters from ~1600 K (the temperature characteristic of both hydrocarbons and their chlorine and fluorine derivatives) to ~1200 K. The kinetic aspects of these studies are presented in detail in [7].

At the same time, a system in which carbon vapor is formed during the pyrolysis of the initial molecules in shock waves would be most attractive for studying the

† Deceased.

0023-1584/01/4205-0583$25.00 © 2001 MAIK "Nauka / Interperiodica"

kinetics of carbon cluster growth. Mixtures containing C_3O_2 can be used for this system. This substance can be considered to be carbon bicarbonyl. At moderately high temperatures, two ligands (CO species) are easily eliminated to form carbon vapor with a high degree of supersaturation, whose subsequent condensation produces particles of condensed carbon.

The main purpose of this work is to study the kinetics of formation of carbon clusters in the pyrolysis of C_3O_2 molecules in shock waves.

EXPERIMENTAL

The kinetics of growth of condensed carbon particles during C_3O_2 pyrolysis behind shock waves was studied using the setup described previously [8]. The yield of condensed carbon particles was determined behind reflected shock waves in a steel shock tube with an inner diameter of 70 mm. The lengths of low- and high-pressure chambers were 4.5 and 3.5 m, respectively. The parameters of the gas behind the shock wave front were calculated from the data on the rate of the incident shock wave [9] measured by piezoelectric sensors. The yield of carbon particles was measured by the absorption of laser radiation (λ = 632.8 and 1064 nm).

Experiments were carried out with mixtures containing 0.03, 0.10, 0.33, and 1.00% C_3O_2 in argon. Hydrogen served as a driver gas. To exclude the effect of hydrogen on the condensation of carbon vapor, we also carried out check experiments where the hydrogen driver gas was replaced by helium. As is known, the following kinetic parameters are usually measured in experiments on soot formation using shock tubes: the induction period τ (time before the beginning of detectable light absorption by carbon clusters), the yield of particles *SY* (ratio of the number of carbon atoms that formed ensembles of condensed particles to the total number of carbon atoms introduced into the reaction zone as constitutients of the starting substance; in this case, each C_3O_2 molecule provides one C atom because two CO ligands are released without decomposition), and the apparent rate constant of cluster growth k_f in the region of the oscillogram whose profile is approximated by the equation

$$SY(t) = SY_\infty[1 - \exp(-k_f t)],$$

where $SY(t)$ is the yield of condensed carbon particles at time t and SY_∞ is the final yield of condensed carbon particles at long times. A typical experimental oscillogram is presented in Fig. 1 (curve *I*) and refers to the conditions of the most intense formation of condensed carbon particles. The very weakly pronounced induction period (the time dependence of the laser-radiation absorption exhibits an *S*-shaped character typical of consecutive reactions) and the good approximation of the main part of the oscillogram by the equation containing the factor $[1 - \exp(-k_f t)]$ are worthy of attention.

The yield of condensed carbon particles was determined from the time dependence of the intensity of the signal of radiation absorption using the following relation:

$$SY(t) = -\frac{\ln(I(t)/I_0(t = 0))}{\alpha d[C_3O_2]_0},$$

where $I(t)$ is the intensity of the absorption signal at time t; $I_0(t = 0)$ is the intensity of the absorption signal at the initial point in time, that is, before the beginning of the thermal decomposition of C_3O_2; α is the absorption coefficient of condensed carbon particles; d is the optical path length of absorbed radiation inside the shock tube; and $[C_3O_2]_0$ is the initial concentration of the starting substance.

However, the absolute values of the resulting *SY* depend substantially on the refractive index n chosen for condensed carbon particles, which in turn depends on the chemical composition of the particles; therefore, in the majority of cases, the exact absorption coefficient of condensed carbon particles is not sufficiently known. In this work, the absorption coefficients for all experiments were chosen equal to 100 (for the laser radiation wavelength λ = 632.8 nm) and 60 m^2/mol (for λ = 1064 nm). In this case, the resulting values of *SY* were always lower than unity.

The processing of oscillograms to obtain parameters τ, k_f, and *SY* is described in detail in [1, 2].

The error of the measurements of the optical absorption signals was ~10–20% depending on experimental conditions. The average error for determining the values τ, k_f, and *SY* was the same. However, at low temperatures, the accuracy of determining these values decreased noticeably because the quasi-stationary level of the absorption signal cannot be determined exactly. Therefore, it is difficult to quantitatively estimate the decrease in the apparent activation energy for k_f at low temperatures.

RESULTS

Figures 2–4 demonstrate parameters τ, k_f, and *SY* in the course of C_3O_2 decomposition plotted against temperature, as determined in this work. They show that the replacement of the hydrogen driver gas by helium left the kinetic parameters of the process almost unaffected.

The yield of condensed carbon particles changed rather weakly with changing the molar fraction of C_3O_2 in the mixture and when the hydrogen driver gas was replaced by helium (Fig. 4). At the same time, the addition of hydrogen to the starting mixture significantly decreased the yield of soot particles, whereas the temperature range of soot formation remained unchanged (Fig. 4, curve *II*).

The condensate remaining on the walls of the shock tube after experiments was analyzed by electron microscopy. It was found that the characteristic size of

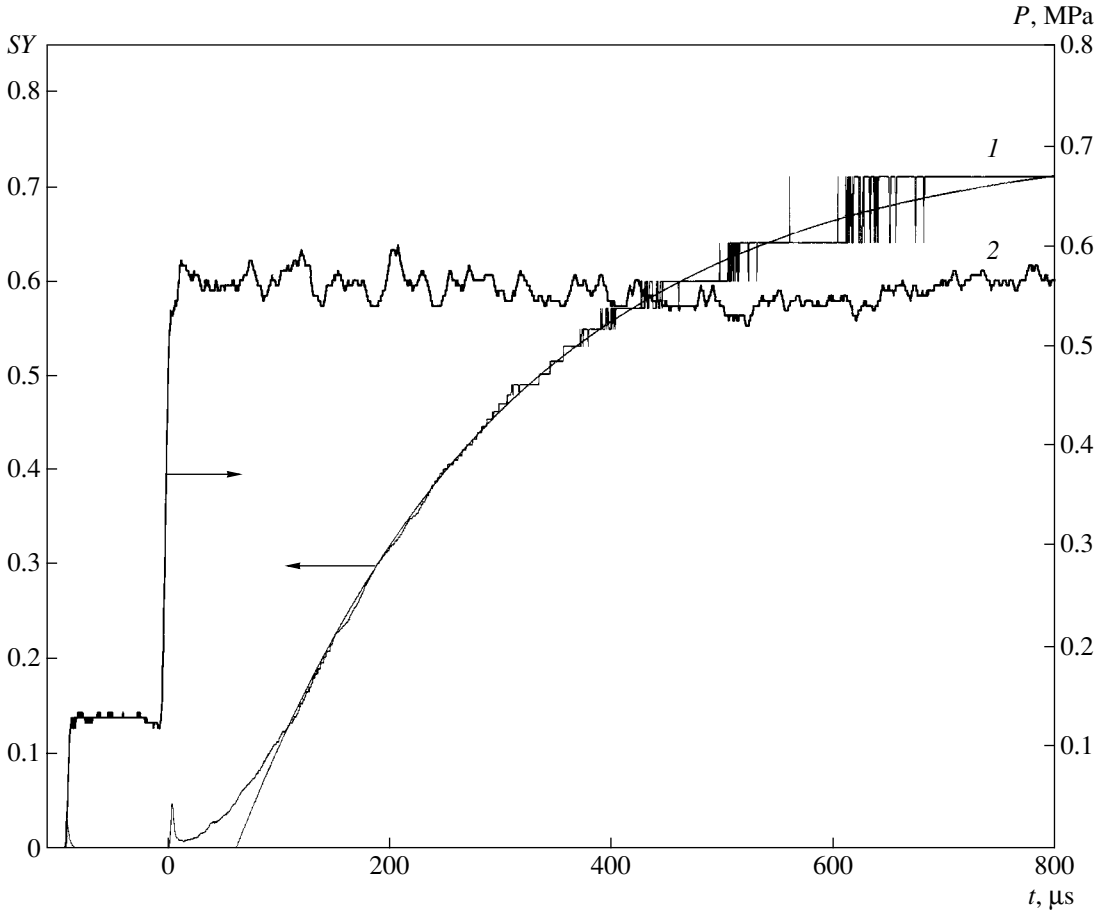

Fig. 1. The profiles of (*1*) laser-radiation absorption by carbon clusters (in *SY* units) and (*2*) pressure behind the shock wave during C_3O_2 decomposition. T_2 = 1673 K; P_2 = 5.56 MPa; a mixture of 0.33% C_3O_2 in argon; driver gas helium; laser-radiation wavelength λ = 632.8 nm. The approximation of the region of the oscillogram of the absorption signal (after the end of the induction period) for the determination of the k_f value is shown in curve *1*.

the particles forming fractal structures was ~30 nm. This value is close to those for particles formed by the pyrolysis of hydrocarbons and their halogen derivatives under similar experimental conditions in shock tubes.

DISCUSSION

The most important qualitative conclusions can be drawn from the above experimental data.

The temperature profile *SY*(*T*) is also characteristic of the majority of test systems [1] but the whole curve is noticeably shifted to low temperatures. This shows that the tendency to condensed carbon particle formation during C_3O_2 pyrolysis is much higher than that for all other systems studied previously.

Let us consider k_f. The absolute values of k_f are much higher than those for any of the studied systems of hydrocarbons or their halogen derivatives. Unlike the latter, in our case, k_f in the Arrhenius coordinates demonstrates a nonmonotonic function of temperature. The absolute values of k_f in the temperature range $T >$ 1500 K ($1/T < 6.7 \times 10^{-4}$) are close to the reduced rate constant of the thermal decomposition of C_3O_2 molecules (Fig. 5). This is the most remarkable property of k_f in the case of cluster formation during C_3O_2 decomposition.

Thus, the formation of condensed carbon particles in C_3O_2 pyrolysis demonstrates interesting kinetic behavior, which was not observed in soot formation during the pyrolysis of structurally different hydrocarbons, including chlorine- and fluorine-substituted hydrocarbons. An important qualitative conclusion on the hierarchy of characteristic times in the test system can be drawn from the closeness of the first-order rate constant of the formation of carbon particles and the reduced rate constant of C_3O_2 decomposition. This coincidence can take place if the growth rate of a condensed phase is much higher than the rate of delivery of the main "building material" for condensate growth. In this respect, the kinetics of formation of condensed carbon particles during C_3O_2 pyrolysis is closer to that of the formation of metal clusters in the pyrolysis of volatile carbonyls rather than to soot formation in hydrocarbon pyrolysis. The type of building material leading to

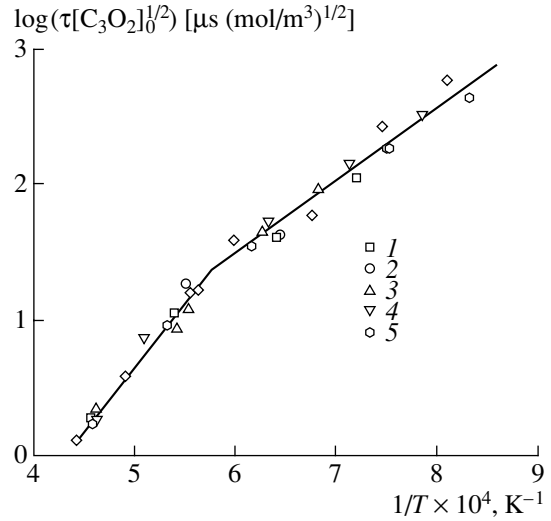

Fig. 2. The temperature dependence of $\log(\tau[C_3O_2]_0^{1/2}$ for soot formation in C_3O_2 pyrolysis. Concentrations of C_3O_2 in argon, vol %: (*1*) 1.00, (*2*) 0.33, (*3*) 0.10 (high-purity argon), (*4*) 0.10, and (*5*) 0.03. (*1*, *3*, *4*, and *5*) driver gas hydrogen; (*2*) driver gas helium.

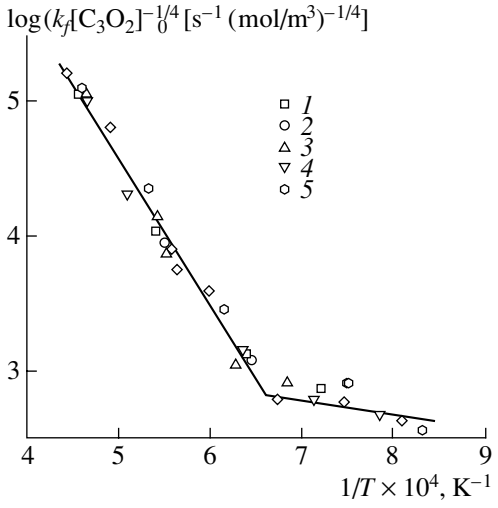

Fig. 3. The temperature dependence of $\log(k_f[C_3O_2]_0^{-1/4}$ for C_3O_2 pyrolysis at the following C_3O_2 concentrations in argon, vol %: (*1*) 1.00, (*2*) 0.33, (*3*) 0.10 (high-purity argon), (*4*) 0.10, and (*5*) 0.03. (*1*, *3*, *4*, and *5*) The driver is gas hydrogen; (*2*) the driver is gas helium.

the growth of carbon clusters is *a priori* unknown; however, different variants can be compared in the framework of appropriate kinetic schemes.

Let us take as a basis the following simplest kinetic scheme composed according to the above concepts:

$$C_3O_2 + M \longrightarrow C_2O + CO + M, \quad \text{(I)}$$

$$C_2O + M \longrightarrow C + CO + M, \quad \text{(II)}$$

$$C + C_3O_2 \longrightarrow C_2 + 2CO, \quad \text{(III)}$$

$$C + C_2O \longrightarrow C_2 + CO, \quad \text{(IV)}$$

$$C_2 + C_3O_2 \longrightarrow N + 2CO, \quad \text{(V)}$$

$$C_2 + C_2O \longrightarrow N + CO, \quad \text{(VI)}$$

$$C + N \longrightarrow N, \quad \text{(VII)}$$

$$C_2 + N \longrightarrow N, \quad \text{(VIII)}$$

$$C_2O + N \longrightarrow N + CO \quad \text{(IX)}$$

(M are particles of the diluent gas, and N are solid carbon particles).

As can be seen, the primary act of C_3O_2 decomposition and the subsequent reactions afford the active fragments C, C_2, and C_2O, which are considered to be the building material for growing condensed carbon particles. For simplicity, it is assumed in the above kinetic scheme that the boundary between nuclei and condensed carbon particles lies in the region of C_3 and the solid carbon particles, which are designated by symbol *N*, in the kinetic scheme grow in reactions involving the active carbon-containing fragments C, C_2, and C_2O. In terms of this simplified kinetic model, the condensed carbon particles are considered in the so-called N-approximation, which only takes into account the growth of the total weight of condensed carbon particles [5].

Unfortunately, in the general case, kinetic equations are awkward expressions, and the corresponding kinetic effects can only be studied by numerical calculations. Nevertheless, we can illustrate the main kinetic regularities using a quasi-steady-state approximation. In this case, the above kinetic scheme for the initial stage of the process under the conditions

$$\frac{k_6[C_2O]}{k_5[C_3O_2]} \gg 1; \quad \frac{k_4[C_2O]}{k_3[C_3O_2]} \gg 1 \quad (1)$$

gives the relation

$$\frac{d(C_s)}{dt} \approx k_1[M][C_3O_2]. \quad (2)$$

Here, $[C_s]$ is the concentration of carbon atoms in the composition of condensed carbon particles, $[C_2O]$ is the quasi-steady-state concentration of C_2O particles, and $[C_3O_2]$ and [M] are the concentrations of the starting substance and the diluent-gas particles, respectively. The apparent rate constant of particle growth k_f (s^{-1}) is equal to $k_1[M]$ in the order of magnitude. Inequalities (1) imply that the reactions of active intermediate species with the starting substance do not substantially accelerate its consumption and do not lead to the autoacceleration of the overall process. It can be expected that at large loads of the starting substance the consumption of the starting substance is accelerated and the apparent rate constant of condensed carbon

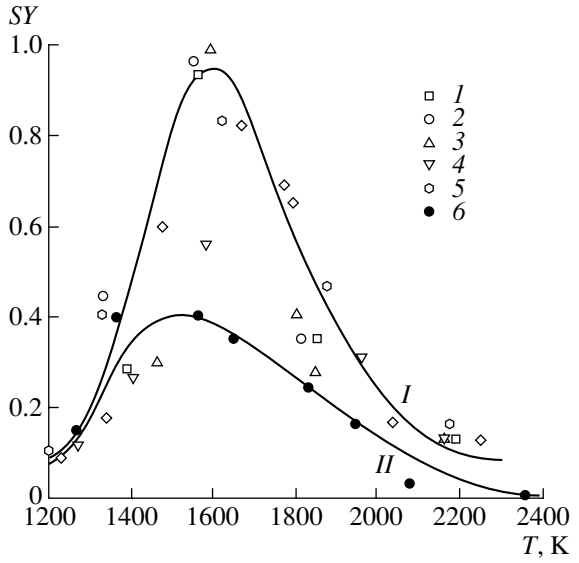

Fig. 4. The temperature dependence of the yield of condensed carbon particles in C_3O_2 pyrolysis in the (*I*) absence and (*II*) presence of H_2 in the reaction mixture. Concentration of C_3O_2 in argon, vol %: (*1*) 1.00, (*2*) 0.33, (*3*) 0.10 (high-purity argon), (*4*) 0.10, (*5*) 0.03, and (*6*) 0.33 (+0.33% H_2). (*1*, *3*, *4*, *5*, and *6*) driver gas hydrogen; (*2*) driver gas helium. Curves *I* and *II* represent the statistical processing of experimental data.

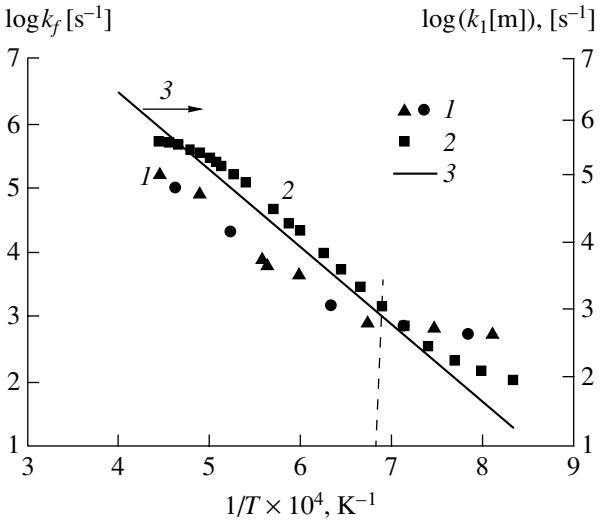

Fig. 5. The temperature dependence of the apparent rate constant k_f of condensed carbon particle growth: (*1*) k_f values obtained from the approximation of the experimental absorption signals at $[C_3O_2]_0$ = 0.10 and 0.33%; (*2*) k_f obtained by the approximation of the calculated plots of the yield of condensed carbon particles using the complete kinetic scheme (Tables 1 and 2); and (*3*) the reduced rate constant of primary C_3O_2 decomposition k_1[m] (the first reaction in Table 1).

particle growth is noticeably higher than the value of k_1[M] for the primary process of starting substance decomposition. The estimations based on scheme (I)–(IX) using the quasi-steady-state approximation show that in calculations the value of k_f can be higher than the value of k_1[M] by a factor of three. This result is consistent with the experimental data (Fig. 5).

Note that the rate constant of the thermal decomposition of C_3O_2 was measured previously [10, 11]. In [10], highly dilute mixtures (about several ppm of C_3O_2 per molecule of the diluent gas) and a highly sensitive resonance absorption technique were used to detect the kinetics of liberation of C atoms. Traditional absorption spectroscopy was used in [11] for C_3O_2 molecules. Because the sensitivity of this method is low, the molar fraction of C_3O_2 in a mixture with Ar was as high as several fractions of a percent. This work is of interest because its authors varied the pressure up to several tens of atmospheres and showed that the decomposition occurred mainly in the low-pressure region or only slightly covered the transition region. The results of measurements in these two works agree well with each other despite significant differences in the measurement techniques, pressure ranges, and molar fractions of C_3O_2 in the mixtures. The main conclusion from a comparison of these works is that the influence of secondary reactions during C_3O_2 decomposition is not too high and the reaction rate is primarily determined by the first stage. This remarkable fact distinguishes C_3O_2 from the entire body of test systems. Note that the previously observed values of k_f did not exhibit any noticeable correlation with the rate constants the of decomposition of parent molecules. In other words, cluster formation in C_3O_2 decomposition shows a close resemblance to the nucleation of vaporous metals formed in the thermal decomposition of carbonyls and other volatile metal-containing compounds in shock waves [12]. The qualitative pattern is reduced to the situation where the rate of carbon cluster growth is limited by the delivery of the building material (C, C_2, …) formed by the decomposition of C_3O_2.

A more complex kinetic model of the formation of condensed particles in C_3O_2 pyrolysis, which gives analytical expressions for the main parameters of the appearance and growth of condensed carbon particles, is based on the consideration of a kinetic scheme of consecutive reactions of the formation and growth of condensed particles [13]. In this case, the model adapted for the considered experimental conditions uses a simplified scheme, according to which the cluster growth is provided by the incorporation of C_2 particles into the C_{2n} cluster and by the reaction of the starting C_3O_2 molecules with the C_{2n} clusters. In this reaction, two CO ligands are released, and the cluster size increases by unity.

Analysis of the kinetic scheme of the consecutive reactions of the formation and growth of condensed

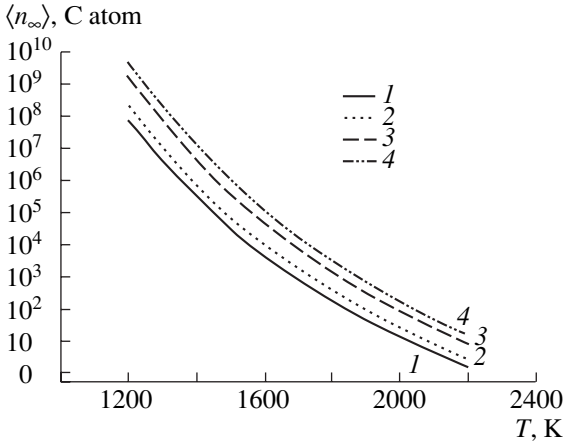

Fig. 6. The temperature dependence of the limiting size of clusters calculated by Eq. (3) for $f_{noneq} = 10.0$ and the activation energies of heterogeneous cluster growth E_a^{het}, kJ/mol: (*1*) 27, (*2*) 42, (*3*) 84, and (*4*) 105.

carbon particles gives the analytical expressions for three important parameters of cluster formation

$$\langle n_\infty \rangle = f_{noneq} \frac{[C_3O_2]_0 k_1^+}{30^{1/2} (k_1)^{3/2}} \exp\left(\frac{E_a^{het}}{2kT}\right), \quad (3)$$

$$T_c = \frac{E_a}{k \ln\{k_1^0 [f_{noneq} \langle n_\infty \rangle_{det} (t_{st})^3 [C_3O_2]_0 k_1^+]^{1/2}\}}, \quad (4)$$

$$t_{cl} = 2.6 \left[\frac{(30)^{1/6}}{f_{noneq}^{1/3}} (k_1)^{1/2} (k_1^+ [C_3O_2]_0)^{2/3} \exp\left(-\frac{7}{6}\frac{E_a}{kT}\right)\right]^{-1}. \quad (5)$$

Here, k is the Boltzmann constant; $\langle n_\infty \rangle$ is the limiting size of clusters; $[C_3O_2]_0$ is the initial concentration of starting molecules; f_{noneq} is the nonequilibrium factor, which indicates the degree of deviation of the rate constant of monomer attachment to clusters from the high-pressure regime and, to a first approximation, is inversely proportional to the Kassel integral used for the approximation of the transition curve from the low-pressure regime to high pressures; k_1 is the rate constant of decomposition of the starting molecule; k_1^+ is the rate constant of monomer attachment to clusters in the limit of high pressures; E_a is the activation energy of unimolecular decomposition of starting molecules; E_a^{het} is the activation energy of heterogeneous cluster growth by the interaction of C_3O_2 with clusters; T_c is the lower boundary temperature for the appearance of clusters; k_1^0 is the pre-exponential factor of the rate constant k_1; t_{st} is the lifetime of steady-state conditions behind the shock wave; $\langle n_\infty \rangle_{det}$ is the sensitivity of the procedure of cluster detection by light absorption; and t_{cl} is the characteristic time of cluster growth. Figure 6 presents the calculated temperature dependence obtained using Eq. (3) for the limit size $\langle n_\infty \rangle$ of cluster at different activation energies of heterogeneous cluster growth and at $f_{noneq} = 10.0$. Figure 7 presents the calculated temperature dependence of the characteristic time of carbon cluster growth obtained using Eq. (5) at different activation energies of heterogeneous cluster growth and at $f_{noneq} = 10.0$. The value of T_c was found from Eq. (4) to be ~1200 K.

This simplified analytical model adequately describes the high-temperature portion of the bell-shaped curve of *SY*. The low-temperature portion gives too high values because it ignores the limiting factor, that is, a finite reaction time (~1 ms) behind the shock wave. As a result, the conversion of the starting molecules in the experiment is low, and the cluster size is also small. From these considerations, Eq. (4) for T_c was obtained.

These concepts allow us to explain qualitatively the formation of a bell-shaped curve for *SY* as a function of temperature. The calculated data for $\langle n_\infty \rangle$ and t_{cl} at $T = 1600$ K agree satisfactorily with the experimental data and the results of numerical calculations according to the complete kinetic scheme (see below).

For the numerical simulation of experimental results on the condensation of carbon formed behind the shock wave front as a result of the thermal decomposition of C_3O_2, we developed a detailed kinetic scheme of possible reactions occurring in this system.

The possibility of the formation of closed spatial structures that consist of five- and six-membered rings is an important element of the kinetic scheme of carbon atom condensation. In this respect, the carbon atom is unique. Clusters of virtually all other studied elements, even beginning already from $n = 10$–13, have an internal atom and then external atomic layers simply grow on the cluster, whereas the situation is different in the case of the carbon atom. Numerous experimental studies of carbon clusters did not find clusters with internal atoms up to $n < 30$–40. Carbon atoms are prone to the initial formation (during condensation) of linear chain structures up to $n = 10$–11, ring and multizing structures at $n = 11$–20, and closed three-dimensional structures consisting of five- and six-membered rings beginning at $n = 30$.

Let us consider briefly the kinetic scheme proposed for the description of carbon condensation during the thermal decomposition of C_3O_2. The scheme contains two main blocks of gas-phase and heterogeneous reactions. Gas-phase reactions include the thermal decomposition of C_3O_2 and the growth and thermal decomposition of small carbon clusters.

In the thermal decomposition of C_3O_2, we consider the formation of C, C_2, and C_2O (Table 1). The rate constants of the main reactions of the thermal decomposition of C_3O_2 and secondary reactions in the kinetic scheme were taken from experimental data obtained in

highly dilute C_3O_2–Ar mixtures [11] and were not changed in calculations.

The reactions involving small carbon clusters (to $n = 10$) include all possible reactions of their growth, coagulation, and thermal decomposition (Table 1). The growth of small clusters involves C_3O_2, C_2O, and C atoms. The decomposition of small clusters (to $n = 10$) is presented by reactions whose activation energies and preexponential factors of the rate constants depend substantially on the cluster size. All possible combinations of coagulating particles to $n = 15$ are considered in the coagulation reactions of small clusters.

The reactions involving larger carbon clusters ($n > 30$) are presented in the block of heterogeneous reactions (Table 2). In this case, particles with $n = 30$ are considered as "nuclei" for future heterogeneous particles and, in essence, combine the blocks of gas-phase and heterogeneous reactions into a single unit.

The growth, coagulation, and structural transformation of heterogeneous particles are considered in the block of heterogeneous reactions. The C, C_2, and C_2O species participate in the growth reactions.

The particles of $C[n] < 70$ (indices in brackets are used to designate the particle size in the solid phase) are considered to be precursors in the formation of soot particles and fullerene-like structures. The particles of $C[n] \sim 70$ can form fullerene-like closed structures with the rate constant characterized by a sharp maximum at the average particle size $C[n] = 70$. These structures need not be fully ordered (in terms of the regular alternation of adjacent five- and six-membered rings) as in the case of fullerenes C_{60} and C_{70}. However, because of the closed three-dimensional structure, they are considered henceforth to be relatively inert species, which do not participate in growth and coagulation reactions.

The particles of $C[n] > 84$ are considered to be soot particles, which participate in growth and coagulation reactions. The C, C_2, and C_2O species participate, as earlier, in the growth reactions.

The size $C[n] = 84$ is conventionally accepted as a boundary between carbon clusters and soot particles. According to this assumption, after the particles reached the average size $C[n] = 84$, they can be transformed into soot particles. The rate constant of this reaction, in the framework of the considered kinetic scheme, is a function of the average particle size and increases sharply from almost zero for $n < 84$ to a certain constant value for $C[n] > 84$.

The complete kinetic scheme of reactions with rate constants used in calculations is presented in Tables 1 and 2 along with references and comments concerning the rate constants used in the calculations.

Taking into account the different optical properties of soot particles and fullerene-like species is an important element for the description of the total experimental yield of particles. Published data [17] indicate a considerable difference in the absorption coefficients of soot particles and fullerenes. The simplest internal normalization procedure was performed as described below to interpret the experimental results of measurements of the absolute value of the total yield of carbon particles. The absorption signal measured at the maximum of the total yield of carbon particles ($T = 1600$ K) was ascribed to the absorption of soot particles, whereas the absorption signal at high temperatures ($T > 2100$ K), which remained almost unchanged with a further increase in the temperature (to $T = 2300$ K), was ascribed to the absorption of fullerene-like species. Due to the fact that we found experimentally that the yield of particles at the maximum is close to 100% and, according to our assumptions, most of the carbon atoms in this case are concentrated in soot particles, we can determine the absolute value of the absorption coefficient of soot particles at a given wavelength. At high temperatures, according to our assumption, most of the carbon atoms are transformed into fullerene-like structures. Measuring the signal of optical absorption at a specific wavelength and associating it with the absorption of fullerene-like structures (in this case, according to our assumption, the yield is also close to 100% in terms of carbon atoms), we can determine the absorption coefficient of fullerene-like species at a specified wavelength of radiation.

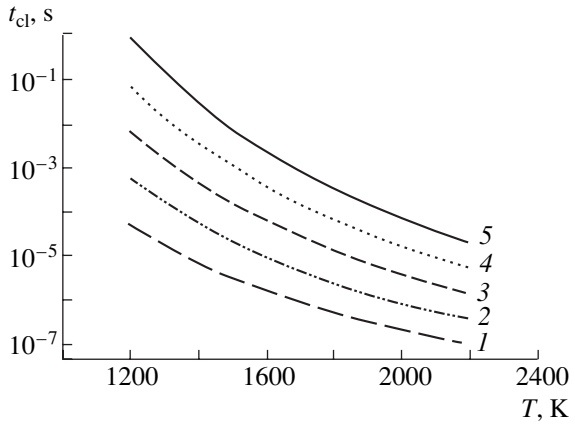

Fig. 7. The temperature dependence of the characteristic time of cluster growth calculated by Eq. (5) for $f_{noneq} = 10.0$ and the activation energies of heterogeneous cluster growth E_a^{het}, kJ/mol: (*1*) 27, (*2*) 42, (*3*) 63, (*4*) 84, and (*5*) 105.

Currently, the most detailed description of the kinetics of transformation of the size distribution function of condensed particles with consideration for various chemical reactions with both gas-phase and heterogeneous condensed components is given by a numerical algorithm based on the discrete Galerkin method [18]. In our case, in the framework of this method, the kinetic scheme formulated above allows the successful description of experimental induction periods for the formation of condensed species due to carbon atom condensation behind the incident shock wave [12] and the total yield of condensed species (Fig. 8).

Table 1. Kinetic parameters of gas-phase reactions

Reaction	Rate constant, $k = A(T)^b \exp(-E_a/RT)$, $cm^3\ mol^{-1}\ s^{-1}$			Notes
	A	b	E_a, kJ/mol	
Thermal decomposition of C_3O_2				
$C_3O_2 + M \longrightarrow CCO + CO + M$	1.5×10^{15}	0.0	245.0	[a]
$CCO + M \longrightarrow C + CO + M$	1.5×10^{17}	0.0	245.0	[a]
$C + C_3O_2 \longrightarrow C_2 + CO + CO$	3.6×10^{14}	0.0	23.0	[a]
$C + CCO \longrightarrow C_2 + CO$	4.5×10^{11}	0.5	0.0	[b]
$CCO + CCO \longrightarrow C_2 + CO + CO$	6.0×10^{12}	0.0	23.0	[c]
$C_2 + CCO \longrightarrow C_3 + CO$	4.5×10^{11}	0.5	0.0	[b]
$C_2 + C_3O_2 \longrightarrow C_3 + CO + CO$	4.5×10^{11}	0.5	85.0	[d]
Growth of small carbon clusters				
$C_n + CCO \longrightarrow C_{n+1} + CO$	4.5×10^{11}	0.5	0.0	$3 < n < 29$[b]
$C_n + C_3O_2 \longrightarrow C_{n+1} + CO + CO$	4.5×10^{11}	0.5	85.0	$3 < n < 29$[d]
$C_n + C1 \longrightarrow C_{n+1}$	4.5×10^{11}	0.5	0.0	$1 < n < 29$[b]
Thermal decomposition of small carbon clusters				
$C_2 + M \longrightarrow C + C + M$	1.2×10^{12}	–1.0	133.98	[e]
$C_2 \longrightarrow C + C$	2.9×10^{15}	0.0	620.12	[f]
$C_3 + M \longrightarrow C_2 + C + M$	1.2×10^{12}	–1.0	184.22	[e]
$C_3 \longrightarrow C_2 + C$	1.9×10^{16}	0.0	737.70	[f]
$C_4 \longrightarrow C_2 + C_2$	3.6×10^{16}	0.0	578.20	[f]
$C_4 \longrightarrow C_3 + C$	5.6×10^{15}	0.0	460.10	[f]
$C_5 \longrightarrow C_4 + C$	1.1×10^{16}	0.0	700.00	[f]
$C_5 \longrightarrow C_3 + C_2$	2.2×10^{16}	0.0	540.50	[f]
$C_6 \longrightarrow C_5 + C$	1.1×10^{17}	0.0	507.90	[f]
$C_6 \longrightarrow C_4 + C_2$	4.2×10^{17}	0.0	588.20	[f]
$C_6 \longrightarrow C_3 + C_3$	1.2×10^{17}	0.0	310.70	[f]
$C_7 \longrightarrow C_6 + C$	1.1×10^{17}	0.0	648.90	[f]
$C_7 \longrightarrow C_5 + C_2$	4.0×10^{18}	0.0	536.70	[f]
$C_7 \longrightarrow C_4 + C_3$	2.4×10^{18}	0.0	499.00	[f]
$C_8 \longrightarrow C_7 + C$	1.1×10^{17}	0.0	531.30	[f]
$C_8 \longrightarrow C_6 + C_2$	3.9×10^{18}	0.0	560.20	[f]
$C_8 \longrightarrow C_5 + C_3$	2.2×10^{19}	0.0	330.30	[f]
$C_8 \longrightarrow C_4 + C_4$	4.5×10^{19}	0.0	570.20	[f]
$C_9 \longrightarrow C_8 + C$	1.1×10^{17}	0.0	646.00	[f]
$C_9 \longrightarrow C_7 + C_2$	3.9×10^{18}	0.0	557.30	[f]
$C_9 \longrightarrow C_6 + C_3$	2.2×10^{19}	0.0	468.50	[f]
$C_9 \longrightarrow C_5 + C_4$	4.3×10^{20}	0.0	515.80	[f]
$C_{10} \longrightarrow C_9 + C$	1.1×10^{17}	0.0	778.30	[f]
$C_{10} \longrightarrow C_8 + C_2$	3.9×10^{18}	0.0	804.30	[f]
$C_{10} \longrightarrow C_7 + C_3$	2.2×10^{19}	0.0	597.90	[f]
$C_{10} \longrightarrow C_6 + C_4$	4.3×10^{20}	0.0	786.30	[f]
$C_{10} \longrightarrow C_5 + C_5$	4.0×10^{21}	0.0	594.10	[f]
Coagulation of small carbon clusters				
$C_2 + C_2 \longrightarrow C_3 + C$	2.5×10^{14}	0.0	74.900	[f]
$C_2 + C_3 \longrightarrow C_4 + C$	2.5×10^{14}	0.0	74.900	[f]
$C_n + C_m \longrightarrow C_{n+m}$	4.5×10^{12}	0.5	0.0	$2 < n, m \le 15$[g]

[a] [11].

[b] The rate constant was chosen by analogy with the rate constant of growth of small carbon clusters, and its absolute value is close to that used in [11].

[c] The parameters involved in the rate constant were similar to those for the rate constant of reaction (4) in [11] with a somewhat decreased preexponential factor.

[d] The activation energy, whose value is typical of reactions between radicals and molecules, was introduced into the rate constant.

[e] The rate constant is similar to that of the reaction of small iron clusters published in [14].

[f] [15].

[g] The rate constant of coagulation was estimated by the method described in [16].

Table 2. Kinetic parameters of reactions involving heterogeneous particles

Reaction	Rate constant, $k = A(T)^b \exp(-E_a^{het}/RT)$, $cm^3\ mol^{-1}\ s^{-1}$			Notes
	A	b	E_a^{het}, kJ/mol	
Formation of nuclei of heterogeneous carbon particles C[$n + m$]				
$C_n + C_m \longrightarrow C[n+m]$*	4.5×10^{12}	0.5	0	$30 \le n + m < 50$[a]
Growth of nuclei of heterogeneous carbon particles C[n]				
$C[n] + C \longrightarrow C[n+1]$	4.5×10^{12}	0.5	0	[b]
$C[n] + CCO \longrightarrow C[n+1] + CO$	4.5×10^{12}	0.5	0	[a]
$C[n] + C_2 \longrightarrow C[n+2]$	4.5×10^{12}	0.5	0	[a]
Coagulation of heterogeneous particles C[n]				
$C[n] + C[m] \longrightarrow C[n+m]$	1.0×10^{12}	0.5	0	[c]
Transformation of heterogeneous nuclei into fullerene species F[n]				
$C[n] \longrightarrow F[n]$	3.0×10^{13}	0.0	300.00	[b]
Transformation of heterogeneous nuclei into soot particles S[n]				
$C[n] \longrightarrow S[n]$	1.0×10^{6}	0.0	0	
Growth of soot particles S[n]				
$S[n] + C \longrightarrow S[n+1]$	4.5×10^{12}	0.5	0	[b]
$S[n] + CCO \longrightarrow S[n+1] + CO$	4.5×10^{12}	0.5	0	[a]
$S[n] + C_2 \longrightarrow S[n+2]$	4.5×10^{12}	0.5	0	[a]
Coagulation of heterogeneous soot particles S[n]				
$S[n] + S[m] \longrightarrow S[n+m]$	1.0×10^{12}	0.5	0	[c]

* The sizes of particles in the solid phase are designated by indices in brackets.
[a] The rate constant was chosen similarly to the rate constant of growth in the reaction with the C atom described in [15].
[b] [15].
[c] The rate constant of coagulation was estimated using the method described in [16].

The experimentally measured apparent rate constants of the growth of condensed carbon species are not described very well; however, a qualitative agreement is also obtained in this case (Fig. 5, points *2*). The most pronounced inconsistency between the measured and calculated k_f values is observed in the middle of the studied temperature range, where the measurement accuracy is highest. The temperature dependence of the average particle sizes of the precursors C[n], the fullerene-like species F[n], and the soot particles S[n] are shown in Fig. 9.

Note that we did not try to achieve the coincidence between the calculated and experimental data on the k_f parameter by varying kinetic coefficients. Evidently, this could be achieved; however, a noticeable deviation of the calculated *SY* and τ plots from experimental data would appear as a result.

At this stage, our approach was to use previously tested individual blocks of reactions without changes for the development of a reasonably full kinetic model and to evaluate its prediction potentialities by the comparison with new experimental data on the kinetics of the liberation of condensed carbon particles.

These blocks are primarily presented by the block of gas-phase reactions for early stages of thermal C_3O_2 decomposition and the block of processes involving fullerenes.

The second parameter, in which the detailed model is noticeably inconsistent with experimental data, is the particle size of condensed carbon formed at the end of the observation of the shock wave. These values are equal to ~10^6 and 10^4 C atoms per particle in the experiment and calculation, respectively. However, note that the particle size and structure of condensed carbon formed behind shock waves should be studied in more detail; this is especially true in regard to the temperature dependence of these parameters. The results of further studies will be published elsewhere.

The analytical model based on the maximally simplified gas-phase kinetic scheme, in which coagulation is neglected (see Eqs. (3) and (4)), results in the remarkable temperature dependence of the maximum particle size and in a correct estimation of the lower temperature limit for the experimental detection of condensed carbon particles. As mentioned above, the limiting particle size of condensed carbon consistent with the

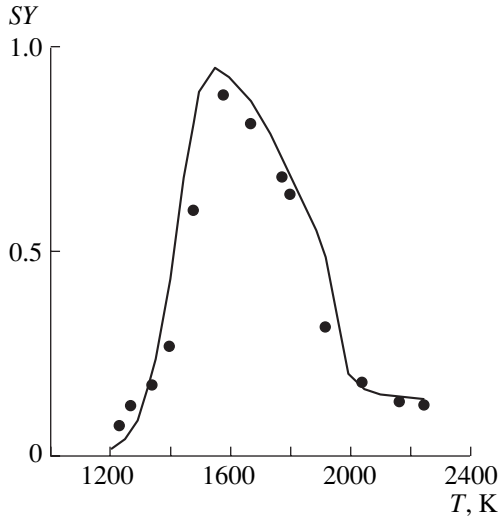

Fig. 8. The temperature dependence of the yield of condensed carbon particles for a mixture of 0.33% C_3O_2 in argon at a pressure of 5.0 MPa and a time of 1×10^{-3} s. Points indicate the result of experimental measurements, solid curve shows the result of numerical calculation.

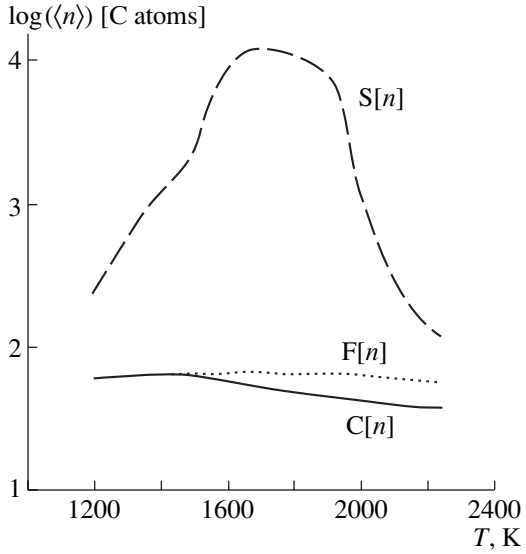

Fig. 9. The temperature dependence of the calculated average particle size of the carbon species C[*n*], F[*n*], and S[*n*] for a mixture of 0.33% C_3O_2 in argon at a pressure of 5.0 MPa and a time of 1×10^{-3} s.

experimental data can be obtained at reasonably chosen free parameters of the analytical model.

Let us emphasize the most important moments that follow from a comparison of the k_f values obtained from the approximation of experimentally measured absorption signals and from the calculated yields of condensed carbon particles as functions of time with the rate constant of the thermal decomposition of C_3O_2 (reaction (I)) at different temperatures. Figure 5 shows that the k_f values obtained by the approximation of the calculated plots of the yield of condensed carbon particles lie much higher than the k_f values obtained by the approximation of the experimentally measured signals of laser-radiation absorption. The temperature plots in the $\log(k_f) - 1/T$ coordinates are obviously nonmonotonic. The deviation from linearity in these coordinates is observed at both low and high temperatures. In the case of low temperatures, this can be related to too long times taken to achieve a quasi-stationary state for experiments in shock tubes and, hence, to a greater arbitrariness in the choice of parameters for approximating the optical absorption curve in this case. From general physical concepts, a deviation at high temperatures also will take place sooner or later. However, it remains unclear at what temperature this will happen. Perhaps, in this case, a limitation is imposed by the approximation procedure itself, the accuracy of the choice of parameters for which also decreases in the case of very fast processes of increasing the front of the optical absorption signal (almost without an induction period). In other words, it is most likely that in the experiment we did not reach the conditions under which the $\log(k_f) - 1/T$ plot will deviate from linearity at high temperatures. Therefore, we can state only a quantitative discrepancy between the k_f values determined from experimental relations and purely by calculations.

Seemingly, the closeness of the calculated values of k_f and k_1[M] (reduced rate constant of C_3O_2 decomposition) is unambiguously indicative of the "simple" kinetics of condensed carbon particle growth when the primary step of C_3O_2 decomposition, which delivers the building material (C_2O) for condensed carbon particle growth, is the rate-limiting step of the growth process. However, as can be seen in Fig. 5, a noticeable difference between the k_f values determined by the calculation (by the complete kinetic scheme) and from experiments suggests a more complex character of condensed carbon particle growth. The possible vibrational superexcitation of carbon clusters during the decomposition of the starting compound and the growth of small carbon clusters is a factor that was ignored in the kinetic simulation of the growth of condensed carbon particles. This superexcitation is possible because all processes of carbon cluster growth are exothermic. The direct experimental observations also demonstrate the "overheating" of C_2 species (these results will be published elsewhere).

During the induction period, the processes of carbon cluster growth are rather slow and close to equilibrium. The effects of vibrational excitation appear only slightly. These processes are most pronounced in the region of the maximum growth rate. Therefore, the τ values and the yields of condensed carbon particles are less sensitive to superexcitation effects.

Returning to the problem of the ratio between experimentally measured k_1 and k_f values, note that the simplest kinetic scheme (see Eqs. (I)–(IX)) gives the correct ratio between them at a knowingly underestimated lower limit of the particle size of condensed carbon with coagulation neglected.

In conclusion, note that the kinetics of condensed carbon particle growth was, in fact, considered in the framework of a spheroid approximation for all models used, and assumptions on chains and planar and closed rings were used only implicitly in the interpretation of thermochemical data. Kinetic deviations from the formalism of the liquid droplet model are of great importance for the description of the processes of formation of carbon nanostructures (fullerenes and nanotubes). However, the problem of taking into account the spatial structure of formed condensed species in kinetic calculations requires further investigations.

ACKNOWLEDGMENTS

We thank Yu.K Karasevich for fruitful discussions, interest in the work, and proposed analysis of the analytical quasi-steady-state kinetic model of carbon cluster growth.

This work was supported by the Russian Foundation for Basic Research (project nos. 98-03-32157, 99-03-32068, and 98-03-04118).

REFERENCES

1. Heynes, B.S. and Wagner, H.Gg., *Progr. Energy Combust. Sci.*, 1981, vol. 7, p. 229.
2. Bauerle, St., Karasevich, Y., Slavov, St., *et al.*, *25th Int. Symp. on Combustion*, Pittsburgh: The Combustion Institute, 1994, p. 627.
3. Frenklach, M., *Chem. Eng. Sci.*, 1985, vol. 40, p. 1843.
4. Krestinin, A.V., *Khim. Fiz.*, 1994, vol. 13, no. 1, p. 121.
5. Zhil'tsova, I.V., Zaslonko, I.S., Karasevich, Yu.K., and Vagner, Kh.G., *Kinet. Katal.*, 2000, vol. 41, no. 1, p. 87.
6. Thienel, T., *Thesis, Russbildung in Der Pyrolyse Hinter Stosswellen. Universitat Gottingen*, 1996.
7. Starikovskii, A.Yu., Thienel, Th., Wagner, H.Gg., and Zaslonko, I.S., *Ber. Bunzen-Ges, Phys. Chem.*, 1998, vol. 102, no. 12, p. 1815.
8. Hwang, S.M., Vlasov, P.A., Wagner, H.Gg., and Wolff, Th., *Z. Phys. Chem.*, 1991, vol. 173, no., p. 129.
9. Gardiner, W.C., Jr., Walker, B.F., and Wakefield, C.B., *Shock Waves in Chemistry*, Lifshitz, A., Ed., New York: Marcel Dekker, 1981.
10. Kijewski, H., Troe, J., and Wagner, H.Gg., *Z. Phys. Chem.*, 1969, vol. 68, nos. 3–6, p. 321.
11. Friederchs, G. and Wagner, H.Gg., *Z. Phys. Chem.*, 1998, vol. 203, no. 1, p. 1.
12. Vlasov, P.A., Zaslonko, I.S., and Karasevich, Yu.K., *Teplofiz. Vys. Temp.*, 1998, vol. 36, no. 2, p. 206.
13. Gordiets, B.F., Shelepin, L.A., and Shmotkin, Yu.S., *Fiz. Goreniya Vzryva*, 1982, vol. 18, no. 2, p. 71.
14. Warnatz, J., Behrendt, F., Sojka, J., *et al.*, *Proc. 3rd Workshop on Modeling of Chemical Reaction Systems*, Heidelberg, 1996.
15. Krestinin, A.V., Moravskii, A.P., and Tesner, P.A., *Chem. Phys. Rep.*, 1998, vol. 17, no. 9, p. 1687.
16. Krestinin, A.V., Smirnov, V.N., and Zaslonko, I.S., *Sov. J. Chem. Phys.*, 1991, vol. 8, no. 3, p. 689.
17. Pierson, H.O., *Handbook of Carbon, Graphite, Diamond and Fullerenes*, Park Ridge: Noyes, 1993.
18. Ackermann, J. and Wulkow, M., *MACRON – A Program Package for Macromolecular kinetics*, Preprint SC 90–14, Berlin: Konrad-Zuse-Zentrum, 1990.